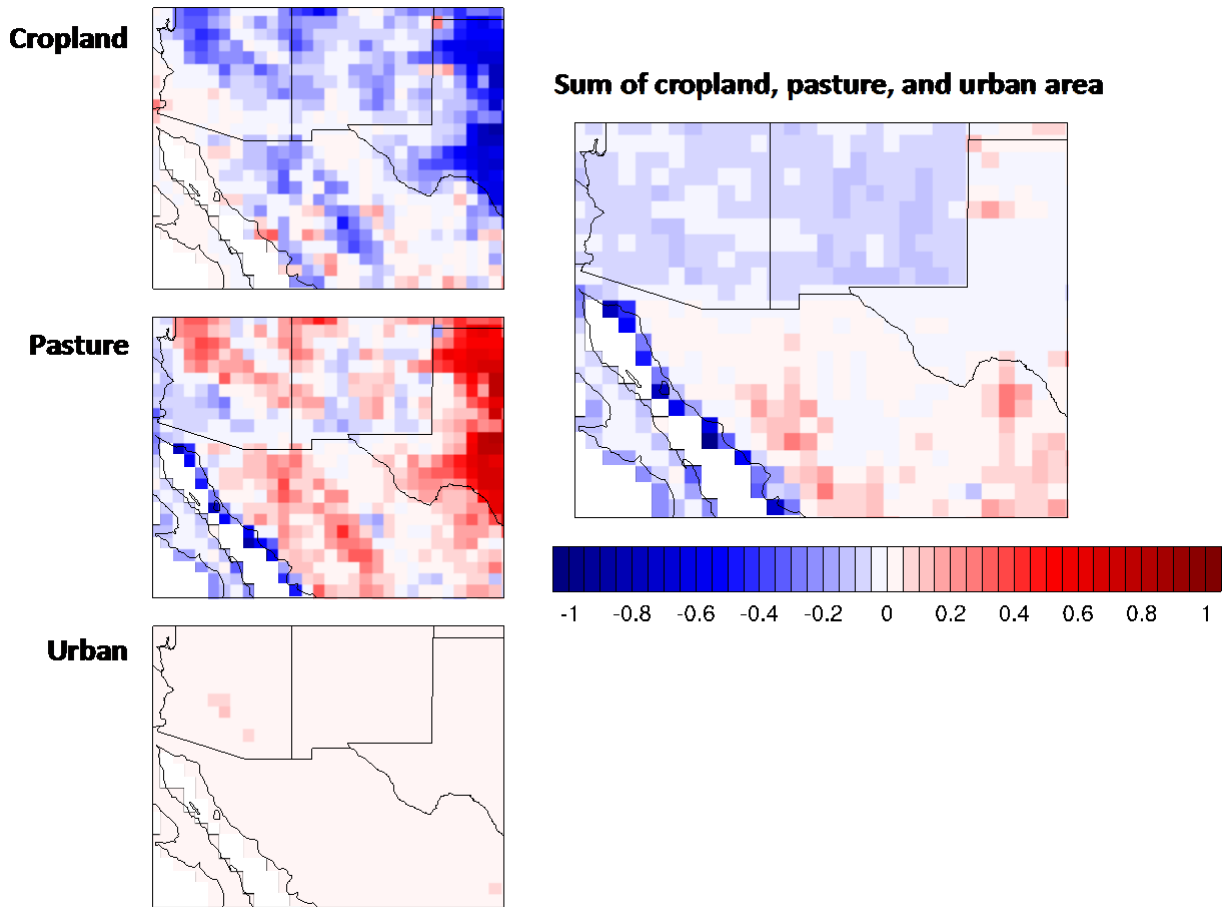Atmospheric
Chemistry
and Physics

Supplement of

Response of dust emissions in southwestern North America to 21st century trends in climate, CO_2 fertilization, and land use: implications for air quality

Yang Li et al.
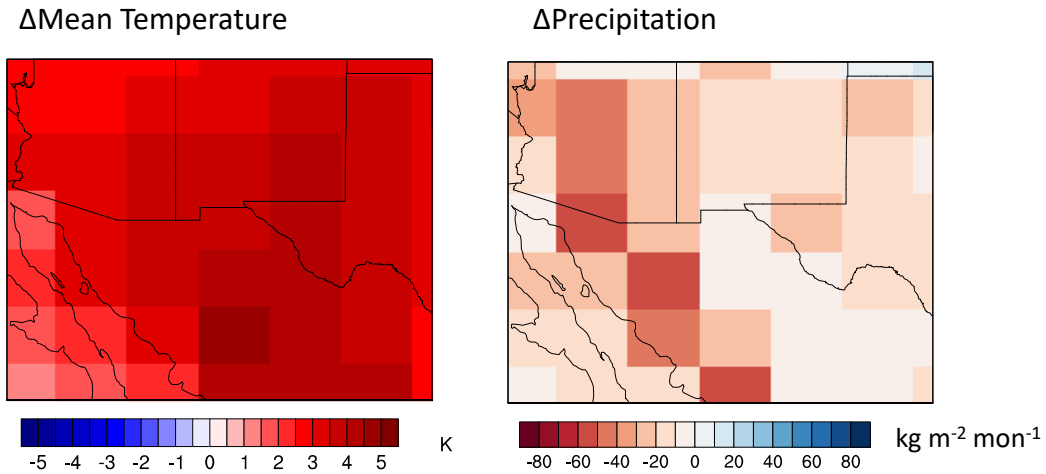
Correspondence to: Yang Li (yangli@seas.harvard.edu)

13

Figure S1. Changes in land use fraction in southwestern North America from 1990 to 2015. Future

land use scenarios applied follow CMIP5. Land use types of cropland, pasture, and urban area are

plotted on the left, and the sum of these three types is plotted on the right.

17

18

ΔMean Temperature · ΔPrecipitation

19

20 **Figure S2.** GISS-E2-R simulated spring averaged monthly mean temperature and precipitation

21 in southwestern North America for RCP8.5. Changes are between the present day and 2100, with

22 five years representing each time period. The color bar is reversed for precipitation, with redder

23 colors indicated drier conditions.

24

25 **Evaluation of dust emissions based on LPJ-LMfire**

26   Figure S3 shows the simulated present-day (2011-2015) distribution of vegetation area

27 index (VAI) over southwestern North America. Values are derived from LAI generated by the

28 LPJ-LMfire dynamic vegetation model, as described in the main text. We find relatively high VAI

29 values in central Arizona, northern New Mexico, northern Texas, and northwestern Mexico, but

30 near-zero VAI in the arid regions of western Texas and along the northern Mexico border. Figure

31 S4 compares the differences in springtime VAI generated by LPJ-LMfire for the present day and

32 that derived from 1-km reflectance data from the Advanced Very High Resolution Radiometer

33 (AVHRR, Bonan et al., 2002). This satellite-based VAI is the default dataset in the DEAD module

34 (Zender et al., 2003). The differences between these two VAI datasets are mostly small, within ± 1

35 m^2 m^{-2}, across southwestern North America, giving us confidence in the performance of LPJ-

36 LMfire. In addition, we categorize the LPJ-LMfire simulated land cover types as trees and shrubs,

37 grasses, and barren land (Figure S5). The high-dust emission region shown in Figure S3 is

38 dominated by grass ecosystems and barren land, roughly consistent with observed land cover

39 shown in the photos of four locations (southwest New Mexico, southeast New Mexico, west Texas,

40 and northern Chihuahua state, Mexico) selected from the principle dust-producing regions in our

41 study (Figure S5).

42   The dominant plant functional types in LPJ-LMfire in the southwestern North America

43 include temperate needleleaf evergreen, temperate broadleaf evergreen, temperate broadleaf

44 summergreen, and C3 perennial grass, roughly consistent with observed, present-day vegetation

45 types (McClaran and Van Devender, 1997). We acknowledge, however, that with only nine PFTs,

46 LPJ-LMfire cannot capture the phenology of all plant species, which could in turn introduce error

47 into our dust calculations. Still, the relatively good match of modeled springtime VAI with that

48 observed is encouraging.

49   Figure S3 also shows the distribution of dust emissions for the present-day RCP4.5

50 scenario, with especially high emissions simulated over those areas with near zero VAI. We apply

51 these emissions to GEOS-Chem and evaluate the resulting fine dust concentrations using ground-

52 based measurements from the Interagency Monitoring of Protected Visual Environments

53 (IMPROVE) network (Malm et al., 2004). Hand et al., 2016 used the observed iron content from

54 IMPROVE as a proxy for fine dust concentrations, and approximated soil-derived $PM_{2.5}$ as $PM_{2.5}$-

55 Iron/0.058. IMPROVE dust observations are made every three days, and we show the spatial or

56 temporal median of these observations as outliers are common in the dataset, and GEOS-Chem is

57 unlikely to capture the extreme dust events. For model validation, we rely on the RCP8.5 results

58   for 2011-2015, which yields nearly identical results as RCP4.5. GEOS-Chem tracks fine dust with

59   a diameter range of 0.2-2.0 μm, while the IMPROVE approximation yields dust concentrations

60   with diameter less than 2.5 μg m^{-3}. This disparity may hinder the model comparison with

61   observations.

62   Figure S6 compares the spatial distribution of GEOS-Chem springtime dust concentrations

63   with observations, and Figure S7 examines the temporal variability of modeled and observed dust

64   averaged over the region. In general, the model captures both the observed spatial and temporal

65   variability, though GEOS-Chem underestimates dust at a few sites in Arizona. This underestimate

66   could be a result of abundant mountain vegetation simulated by LPJ that alleviates dust generation

67   from persistently arid or desert regions. The 2011-2015 timeseries of observed and modeled dust

68   (Figure S7) reveals that GEOS-Chem exhibits a smaller seasonal variation of 0.2-3.1 μg m^{-3},

69   compared with the observed range of 0.2-8.1 μg m^{-3}. Overall, we find that the present-day

70   simulations reasonably reproduce observed fine dust over southwestern North America.
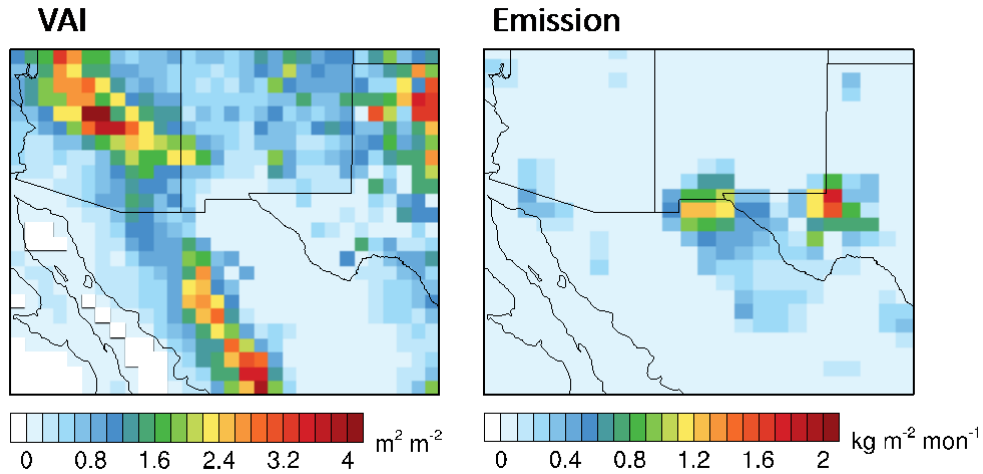
Figure S3. Present-day (2011-2015) spring averaged VAI and fine dust emissions for the RCP8.5 fixed-CO_2 case in southwestern North America, in which CO_2 fertilization is neglected. VAI results are from LPJ-LMfire. Dust emissions are generated offline using the GEOS-Chem emission component (HEMCO).
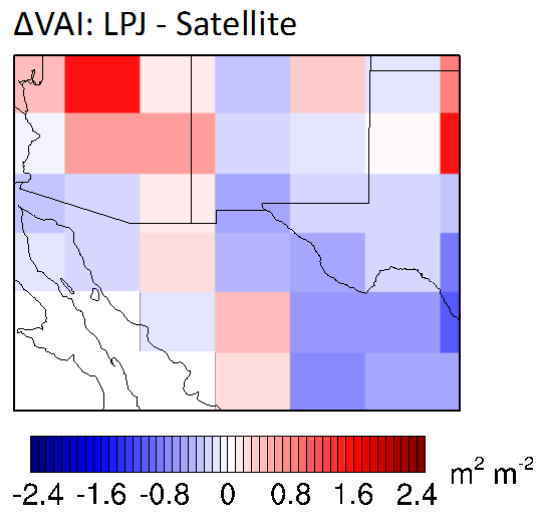
Figure S4. Differences between springtime VAI simulated by LPJ-LMfire and that derived from 1-km satellite data in southwestern North America. The LPJ-LMfire results are the mean 2011-2015 values from the RCP8.5 fixed-CO_2 case; satellite-derived VAI are from Bonan et al. (2002).

81

Tree cover   Grass cover   Unvegetated
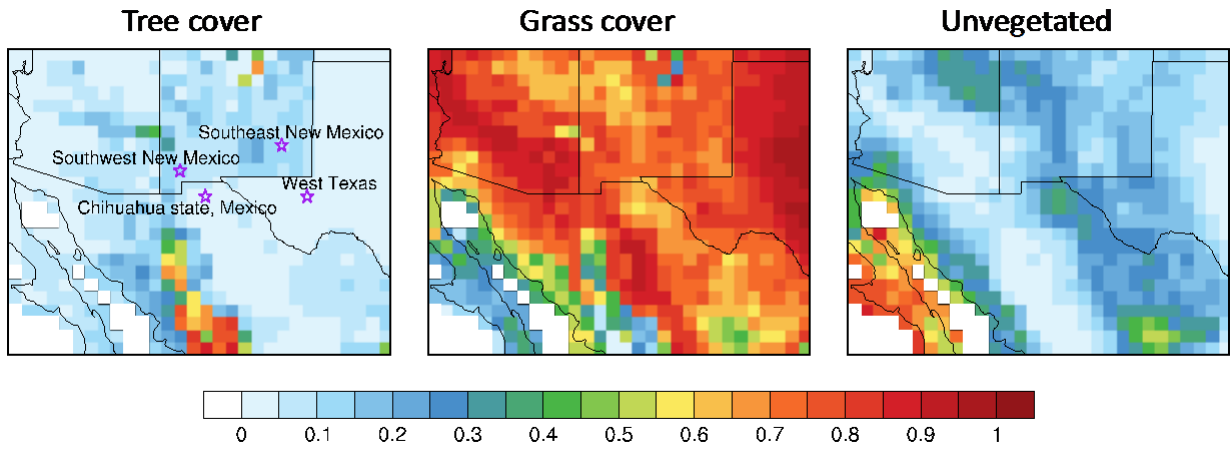
82

103.25°W 31.25°N (West Texas)
LPJ: 0.3% trees/shrubs, 74.9% grass, 24.8% unvegetated
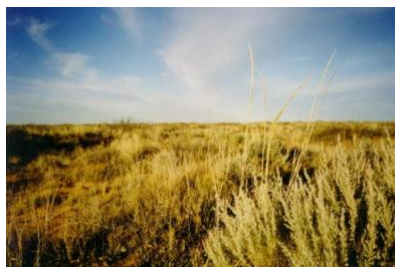

The Degree Confluence Project, 2011   Google Street View, 2013   The Degree Confluence Project, 2011

104.25°W 33.25°N (Southeast New Mexico)
LPJ: 0.5% trees/shrubs, 73.4% grasses, 20.1% unvegetated

83

The Degree Confluence Project, 1999   Google Street View, 2013   Google Street View, 2013

108.25°W 32.25°N (Southwest New Mexico)
LPJ: 12.7% trees/shrubs, 73.3% grasses, 14.0% bare ground

Google Street View, 2014 · The Degree Confluence Project, 2014 · The Degree Confluence Project, 2014
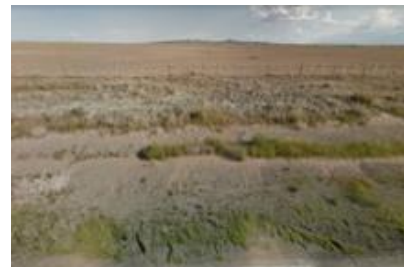
107.25°W 31.25°N (Chihuahua state, Mexico)
LPJ: 2.4% trees/shrubs, 65.3% grasses, 32.2% bare ground

The Degree Confluence Project, 2005 · Google Street View, 2019 · Google Street View, 2018

Figure S5. Top panels show mean fractional land cover of trees, grasses, and barren land averaged over 2006-2015, as simulated by LPJ-LMfire. Purple stars on the top lefthand panel mark four selected locations that are broadly representative of vegetation within the principle dust-producing regions in our study, with photographs of each location shown below. Latitude and longitude values listed above each row of photographs denote the center of the LPJ-LMfire gridcell, and the corresponding photographs are all taken within the area encompassed by the 0.5° × 0.5° gridcell. Credits for photographs from t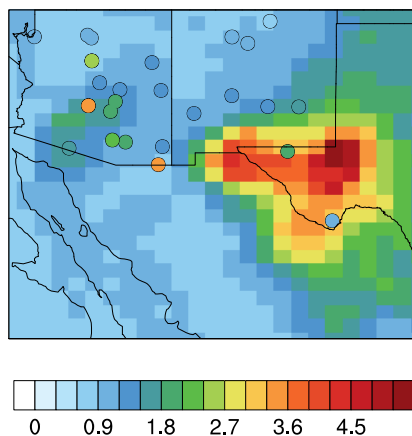he Degree Confluence Project (www.confluence.org) are as follows: Alan B. (west Texas), Matt Taylor and Scott Kessel (southeast New Mexico), Jerry Heikkinen and Shawn Fleming (southwest New Mexico), and Luis Baca (Chihuahua, Mexico).
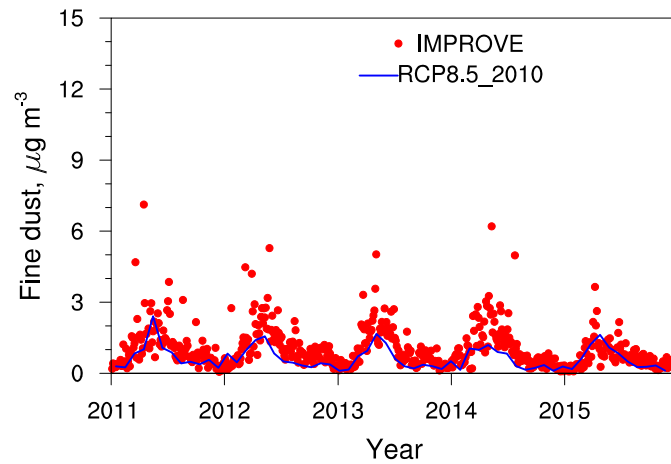
95

96

Figure S6. Spring fine dust concentration. Circles represent ground-based observations from the
IMPROVE network, shown as the medians at each site over 2011-2015. The colored background
is from GEOS-Chem simulations with the present-day (2011-2015) fine dust emissions for the
RCP8.5 fixed-CO_2 case at 0.5° x 0.625° spatial resolution.

101

102

103

Figure S7. Seasonal cycle of GEOS-Chem simulated and IMPROVE observed fine dust

concentrations, shown as the medians over southwestern North America from 2011 to 2015. The

red dots represent the median of IMPROVE observations taken over all sites in the region at each

measurement timestep. IMPROVE has a measurement frequency of every three days. The solid

line shows GEOS-Chem simulated variations at 0.5° x 0.625° resolution for the 2010 time slice

for the RCP8.5 fixed-CO_2 case.

110

111
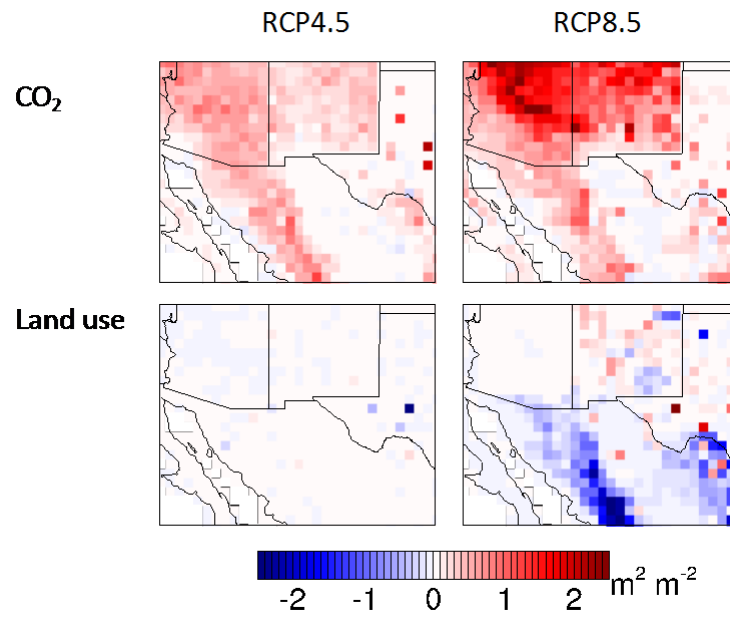
Figure S8. Contributions of CO_2 fertilization and anthropogenic land use to changes in VAI in

spring in southwestern North America for RCP4.5 and RCP8.5. Changes are between the present

day and 2100, with five years representing each time period. The top row is for CO_2 fertilization,

and the bottom row is for land use trends. Results are from LPJ-LMfire.

116

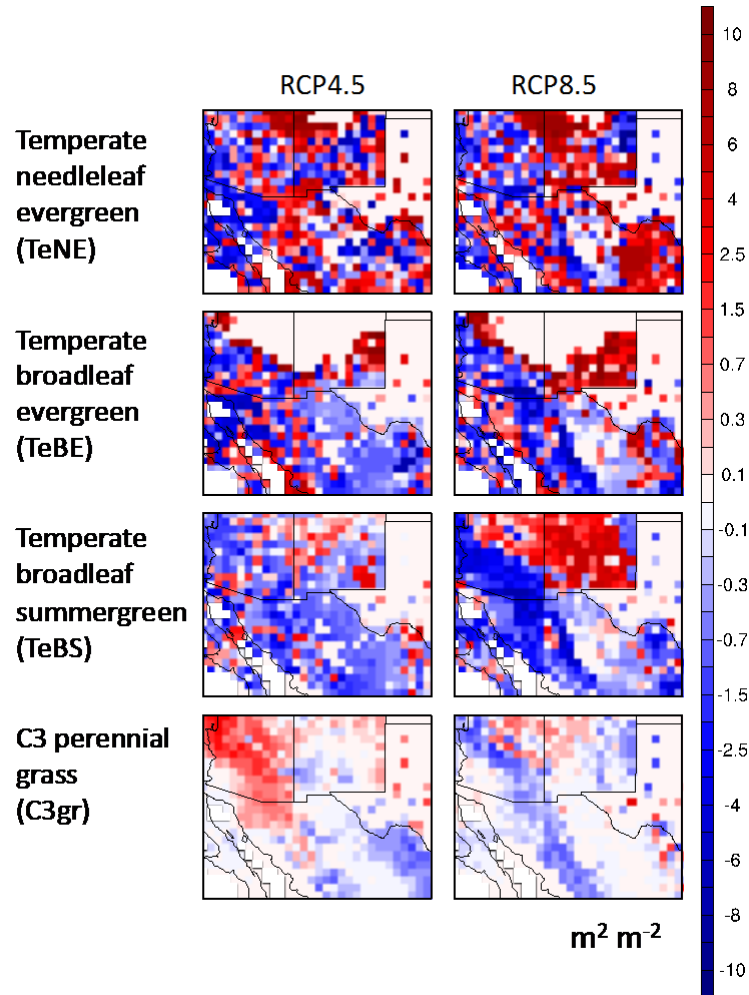RCP4.5   RCP8.5
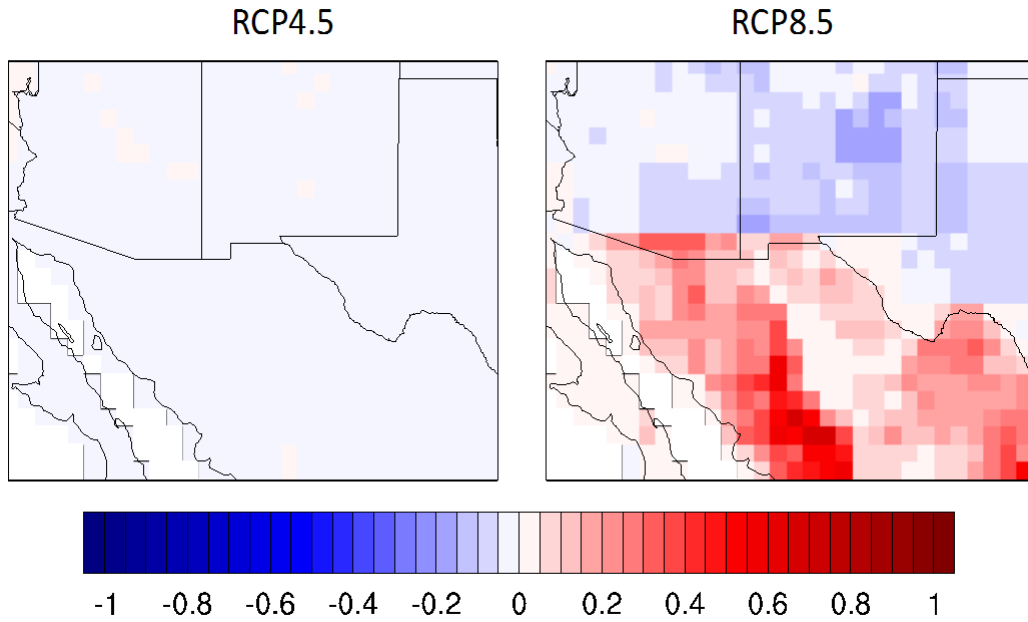
117

118   **Figure S9.** Changes in yearly averaged land use fraction in southwestern North America for

119   RCP4.5 and RCP8.5 between the present day and 2100, with five years representing each time

120   period. Future land use scenarios applied follow CMIP5. Land use plotted here is the sum of

121   cropland, pasture, and urban area.

122

Figure S10. Simulated changes in springtime averaged LAI for the four dominant plant functional types (PFTs) in southwestern North America under RCP4.5 and RCP8.5 for the fixed-CO_2 condition, in which CO_2 fertilization is neglected. Changes are between the present day and 2100, with five years representing each time period. For clarity, the increments in the color bar are unevenly distributed. Results are from LPJ-LMfire.

133 **References**

134 Bonan, G. B., Levis, S., Kergoat, L., and Oleson, K. W.: Landscapes as patches of plant functional
135   types: An integrating concept for climate and ecosystem models, Global Biogeochemical Cycles,
136   16, 5-1-5-23, 2002.
137 Hand, J., White, W., Gebhart, K., Hyslop, N., Gill, T., and Schichtel, B.: Earlier onset of the spring
138   fine dust season in the southwestern United States, Geophysical Research Letters, 43, 4001-4009,
139   2016.
140 Malm, W. C., Schichtel, B. A., Pitchford, M. L., Ashbaugh, L. L., and Eldred, R. A.: Spatial and
141   monthly trends in speciated fine particle concentration in the United States, Journal of
142   Geophysical Research: Atmospheres, 109, 2004.
143 McClaran, M. P., and Van Devender, T. R.: The desert grassland, University of Arizona Press,
144   1997.
145 Zender, C. S., Bian, H., and Newman, D.: Mineral Dust Entrainment and Deposition (DEAD)
146   model: Description and 1990s dust climatology, Journal of Geophysical Research: Atmospheres,
147   108, 2003.
148